A Reverse Compensation Framework for Shape Deformation Control in Additive Manufacturing

Kai Xu
Epstein Department of Industrial and Systems Engineering,
University of Southern California,
Los Angeles, CA 90089

Tsz-Ho Kwok
Epstein Department of Industrial and Systems Engineering,
University of Southern California,
Los Angeles, CA 90089

Zhengcai Zhao
Epstein Department of Industrial and Systems Engineering,
University of Southern California,
Los Angeles, CA 90089

Yong Chen[1]
Epstein Department of Industrial and Systems Engineering,
University of Southern California,
Los Angeles, CA 90089
e-mail: yongchen@usc.edu

Shape deformation is a well-known problem in additive manufacturing (AM). For example, in the stereolithography (SL) process, some of the factors that lead to part deformation including volumetric shrinkage, thermal cooling, added supporting structures, and the layer-by-layer building process. Variant sources of deformation and their interactions make it difficult to predict and control the shape deformation to achieve high accuracy that is comparable to numerically controlled machining. In this paper, a computational framework based on a general reverse compensation approach is presented to reduce the shape deformation in AM processes. In the reverse compensation process, the shape deformation is first calculated by physical measurements. A novel method to capture the physical deformation by finding the optimal correspondence between the deformed shape and the given nominal model is presented. The amount of compensation is determined by a compensation profile that is established based on nominal and offset models. The compensated digital model can be rebuilt using the same building process for a part with significantly less part deformation than the built part related to the nominal model. Two test cases have been performed to demonstrate the effectiveness of the presented computational framework. There is a 40–60% improvement in terms of L^2- and L^∞-norm measurements on geometric errors. [DOI: 10.1115/1.4034874]

Keywords: additive manufacturing, reverse compensation, shape deformation, parameterization, stereolithography

1 Introduction

The use of additive manufacturing (AM) in fabricating near-net shape components is limited by the attainable accuracy of AM processes. For example, the mask-image-projection-based stereolithography (MIP-SL) process using digital micromirror device (DMD) [1] can selectively cure resin to accumulate desired shapes using mask images [2,3]. Several mask image planning methods have been developed to facilitate this process [4,5]. Although the MIP-SL process has advantages such as high fabrication speed [6,7] and resolution [5], the built parts have shape deformation after they are removed from the building platform. Figure 1 shows an example of such deformation, in which a flat rectangular bar that was built by the MIP-SL process is shown. From the figure, it can be seen that the built object is not flat. This is due to the anisotropic deformation that makes the shape curl when compared to the original nominal model (shown in the dashed line in Fig. 1). This kind of shape deformations is common in the parts built by the AM processes. The goal of the paper is to develop a general computational framework to reduce the shape deformations in the AM processes. Without loss of generality, our discussion will be based on the MIP-SL process. However, the presented computational framework is general and can be used to reduce part deformation in other AM processes as well.

Stereolithography (SL) is a complex chemical reaction process, in which liquid monomers are cross-linked into solid polymer under light exposure [8]. The reasons that cause shape deformation come from several aspects as summarized in Fig. 2. First, intrinsic volumetric shrinkage takes place when resin is converted from liquid to solid. Different photocurable resins may have varying volumetric shrinkage rates. The liquid resin commonly used in the MIP-SL process is acrylate, which has a larger shrinkage rate than epoxy used in the laser-based SL process [9,10]. Hence, the deformation in the MIP-SL process is more challenging. Second, photopolymerization process is an exothermic reaction process, in which heat will be generated, and the fabricated part will undergo thermal shrinkage when the cured layers cool down [11,12]. Some

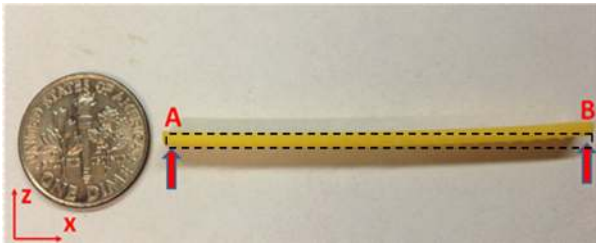

Fig. 1 An example of a physical object built by the MIP-SL process that deforms when compared to the nominal shape

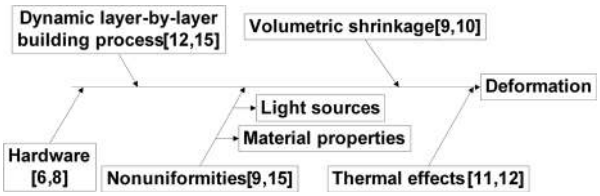

Fig. 2 Deformation sources

[1]Corresponding author.

Contributed by the Computers and Information Division of ASME for publication in the Journal of Computing and Information Science in Engineering. Manuscript received July 22, 2016; final manuscript received August 28, 2016; published online February 16, 2017. Editor: Bahram Ravani.

researchers have used IR cameras to study the curing temperature in the MIP-SL process [13,14]. Third, the additive manufacturing processes build part on a layer-by-layer basis, and the shrinkage of current layer is restricted by the underlying layers. Consequently, residual stress builds up when current layer shrinks [12,15]. Generally, the MIP-SL process can be categorized into two types: constrained-surface and free-surface, which exert different constraints on the curing layers during the building process [6,8]. Besides, the nonuniformities of light source and material properties may also contribute to the deformation since these nonuniformities lead to varying curing rate of resin and thus nonuniform shrinkage [9,15]. Moreover, variants of MIP-SL process and hardware setup may play a role in the final shape deformation.

1.1 Related Works. Deformation control is a critical challenge for additive manufacturing processes. Extensive researches have been conducted on improving the part accuracy in AM processes including the SL process. Some previous research tried to reduce the deformation in the process planning, e.g., to explore different building styles that can reduce the internal stresses induced in the building process [16,17]. In our previous work, we reported using several exposures to cure a layer, which can effectively reduce volumetric shrinkage and lower the curing temperature during the photopolymerization process [13,14,18]. Some other researchers employed design of experiments (DOEs) to study effects of key building parameters, and optimize them in order to reduce deformation of built parts [19,20]. However, even being reduced, shrinkage and internal stresses still exist in the building process, since the phase change of material takes place in AM processes, and parts are built in a layer-by-layer dynamic style.

Some researchers used either finite-element method (FEM) or analytical methods to model the SL process [9,12,21]. However, as illustrated in the introduction, many factors contribute to the final deformation. It would be rather difficult to incorporate all the factors in the finite element analysis (FEA) simulation to get good predictions. Some researchers studied shape compensation instead of reducing the deformation in the fabrication process. For instance, Huang and Lan [22] used FEA simulation to predict the distortion of part and calculated the dynamic reverse compensation by considering the distortion of added compensation. Tong et al. [23] presented a method to transfer all errors sources in AM process into parametric error functions. Errors were predicted by the parametric error functions, and original computer-aided design (CAD) model was compensated by applying negative values of errors. Zha and Anand [24] presented a geometric approach to improve errors of part by modifying input stereolithography (STL) models in AM processes. Huang et al. [25–27] conducted research using statistical approaches to model and predict in-plane shrinkage and out-of-plane deformation of different parts, and derive compensation to improve accuracy of built part in the MIP-SL process. All these research have effects on improving errors of built parts in AM processes. However, some limitations need to be addressed. (1) Deformation based on predictions using FEA simulation is not accurate since it is difficult to incorporate all deformation sources in the simulation. (2) Modifying the original STL model by directly adding the predicted error reversely on the vertices is inaccurate since the added compensation also contributes to the final deformation. And (3) it is difficult to predict complex shape using statistical model, which may need extensive experimental data.

1.2 Contributions. Due to the fact that the shape deformation of a fabricated part comes from many different sources and their complex interactions, it is difficult to predict and compensate all the factors one by one. Instead, our research proposes a general reverse compensation framework, in which all the factors are combined to a geometric design problem by assuming the parts are fabricated using the same manufacturing process. Thus, the "law" of shrinkage is preserved for the given shape. Specifically, we fabricate the given nominal model and some designed offset models to identify the relationship between the shape and its related deformation. Accordingly, we modify the input geometry such that the modified shape can be fabricated using the same building process to fabricate a part that is much closer to the nominal model. Our contributions can be summarized as follows:

- A general computational framework for compensating the fabrication error is presented by converting the complex sources of deformation to a geometry optimization problem;
- A continuous mapping method based on cross-parameterization is established to capture the physical deformation of the fabricated models;
- An approach of estimating required compensations by studying the nonlinear relationship between the given shape and its related deformation based on building the nominal and offset models.

The rest of paper is organized as follows. Section 2 presents an overview of the proposed compensation framework. Section 3 explains the computation of correspondence between two models and the calculation of related deformations. Section 4 introduces the compensation estimation based on the calibration of nominal and offset models. Two test cases are demonstrated and analyzed in Sec. 5. Finally, conclusions are drawn in Sec. 6 with future work outlined.

2 Overview of Reverse Compensation Framework

Figure 3 shows the computational framework for reducing deformation in AM processes. Any built parts with deformations that exceed required tolerance can use this computational framework to reduce the fabrication deformation.

In order to reduce the undesired shape deformation, the first step is to capture it. As deformation is difficult to predict accurately by analytical models or FEM simulation, we adopt the approach of measuring deformation based on physical measurement using tools such as coordinate measurement machines (CMMs) or 3D scanners. After the fabricated object is measured, the correspondence between a set of points on the nominal model and the measured one needs to be established. In this research, we designed artificial markers in the nominal shape, and use them and other feature points to establish the correspondence between input and fabricated models. Based on the established

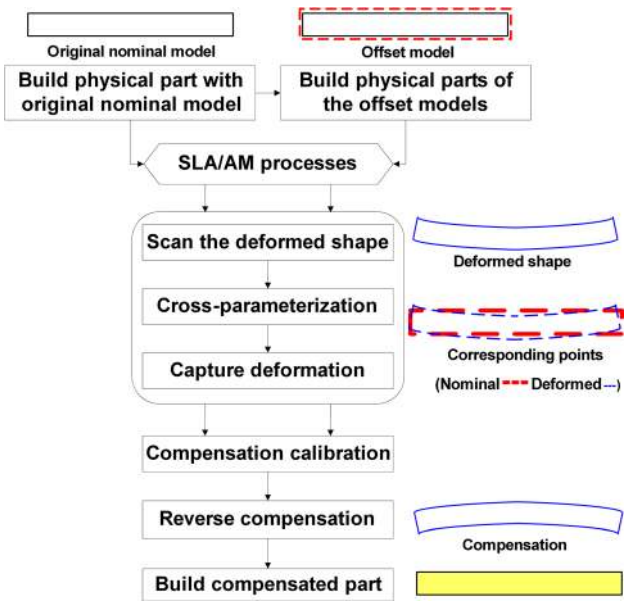

Fig. 3 A computational framework to reduce shape deformation in AM processes

correspondence, the two models can be aligned; hence, the deformation can be calculated by subtracting the coordinates of corresponding points on the two models. After the deformation is calculated, a reverse compensation approach is used to modify the nominal model such that the built part would be closer to the designed nominal model. The schematic of a test case using a simple bar is shown in Fig. 3 to illustrate the reverse compensation method. As shown in Fig. 1, the original flat simple bar has deformation after built, and the two tips curl up. We can use a CMM to measure its deformed profile. The correspondence between the measured deformed profile and original nominal profile is established. For each point on the nominal model, a corresponding point can be found on the deformed profile. The deformation for each point on the nominal model is calculated by subtracting its coordinates from the corresponding point on deformed profile. Additional offset models are designed by adding small compensation along the normal direction of each point on the original nominal model (one example of such offset models is shown in dashed line, with the solid line being the original nominal model). They are also built and measured following the same procedures as the original nominal model. The relations between added offsets (compensation) and resulted deformation are explored to provide compensation profile of the given shape. The nominal STL model can be modified by using the reverse compensated profile, and the modified STL model is rebuilt for a final built that is much closer to the nominal shape.

Specifically, the compensation for each point can be calculated based on the deformation of nominal and offset models. Pick a random point P on the original nominal model as an illustration. Let the added compensation to be X, and the deformation of the compensated point $(P+X)$ is denoted as $f(P+X)$, which is a function of added compensation X. The objective of compensation is to find X so that

$$P + X + f(P + X) = P \tag{1}$$

It can be rewritten as

$$X + f(P + X) = 0 \tag{2}$$

To solve this equation, there are two main issues that have to be tackled.

(1) Given the nominal and the deformed models, how to capture the physical deformation for every point on the models, such that f can be computed for a particular P?
(2) As $f(P+X)$ is a function of X, the relation between X and $f(P+X)$ is unknown and nonlinear. How to find the value of X such that it can satisfy or better approximate Eq. (2)?

These two questions will be answered in Secs. 3 and 4. Before that, we define the following notions that will be used in the paper:

N is the nominal model, which is the CAD model that needs to be fabricated, M is the measured data of the fabricated physical model, which has undergone deformation, C is the compensated CAD model, $N_{\pm}$ is the subscript + or − denotes the offset version of the model, i.e., outward or inward, respectively.

3 Correspondence and Deformation of Design and Fabrication Models

To capture the deformation of each point on the nominal model (N) such that the deformation function f can be computed, we need to find its corresponding point in the deformed physical model (M). One way to find the corresponding points is using the closest points like in the iterative closest point method [28]. However, using closest points cannot capture the real physical deformation, because it may lead to a many-to-one or one-to-many mapping that will result in degenerated shapes, which is not likely to happen in the physical case. It is hard to find a mathematical model that is consistent to the physical deformation; however, we believe a smooth mapping with minimized stretching distortion can mimic the physical deformation well, since the stretches and tensions caused by shape deformation are generally distributed on the surface of the physical model. Therefore, we establish these correspondences using a smooth mapping based on cross-parameterization; in addition, designed features are incorporated to improve the accuracy of the correspondences. The details of which will be described in this section.

3.1 Establishing Correspondence Between Models. In our study, we establish the correspondence between nominal model (N) and deformed model (measured model, M), as well as for nominal model (N) and offset models (N_+, N_-), by using feature points that are known to have correspondence on two models. This can be done either by manual specification or by some intelligent feature recognition algorithms [29]. If there is no salient feature point on some model surfaces, we add artificial markers on the surfaces to serve as the feature points. An illustration of added markers is shown in Fig. 4. The markers are desired to be small to have minimum effect on the fabrication process; at the same time, the markers cannot be too small in order for them to be successfully built and measured. Based on our tests, we designed the markers as a set of cylinders with a diameter of 0.6 mm and a height of 0.5 mm.

The specified feature points define a sparse and discrete correspondence among different models. To establish a continuous mapping from the sparse correspondence, we apply the cross-parameterization method [30,31]. Specifically, the method partitions both of the models to a set of corresponding patches by linking the input feature points in a consistent way. Accordingly, the cross-parameterization between the models is found by computing the mapping between all the corresponding patches. The mapping computed is bijective and optimized to have low distortion. Due to reason that the cross-parameterization is computed based on the Voronoi diagram on the surface of the model with the markers as the seeds, it is suggested that markers should be placed uniformly on the model such that the Delaunay triangulation dual to the diagram is regular. An example of cross-parameterization result is shown in Fig. 5, in which 35 artificial markers have been added, respectively, on the two models.

3.2 Capturing the Deformation of Physical Model. Once the correspondence between the nominal model (N) and the deformed physical model (M) is established, they can be aligned, and the deformation for each point on the nominal profile can be calculated by subtracting its coordinate from that of its corresponding point on the measured profile.

For an illustration, a modified letter H model is widely used for the accuracy study in the SL process. The schematics of the model used in our study are shown in Fig. 6 (unit in mm). The part has

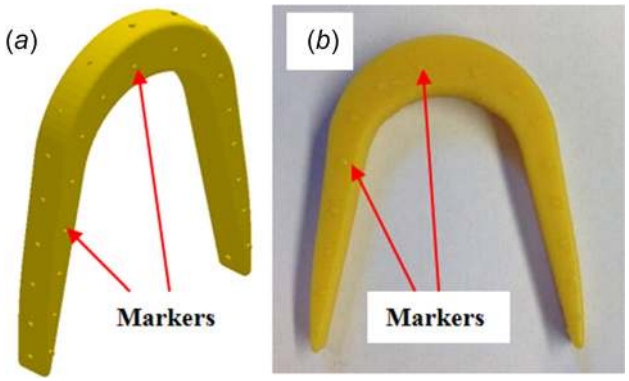

Fig. 4 Models with no salient feature points (*a*) nominal CAD model and (*b*) built physical model

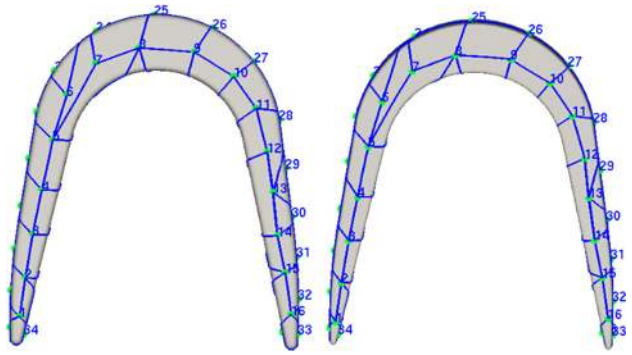

Fig. 5 Cross-parameterization of two models with 35 artificial markers

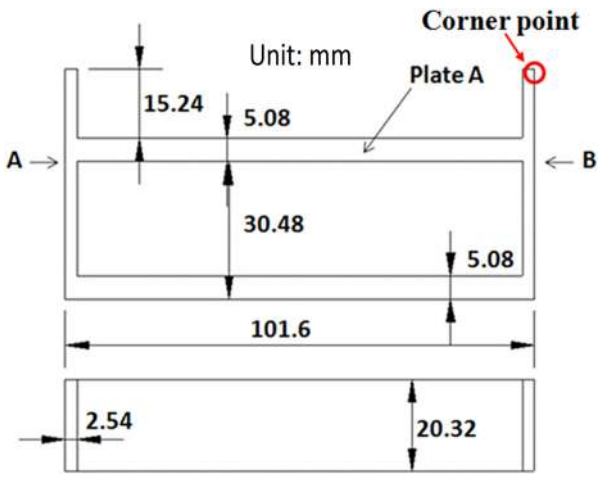

Fig. 6 Schematic of modified letter *H* part

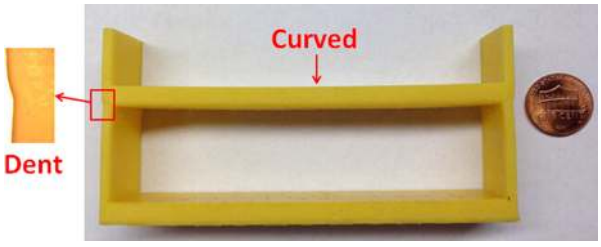

Fig. 7 Built object of the modified letter *H* model

length of 101.6 mm, width of 20.32 mm, and height of 50.8 mm. The model was built using a commercial MIP-SL machine (Ultra by EnvisionTec, Inc. [3]). The built object is shown in Fig. 7. It can be observed that plate A is curved, and points A and B have dents on the vertical surfaces due to volumetric shrinkage.

As the modified letter H part is a 2.5D model, we can measure its 2D profile using a vision-based measurement tool. In this research, a high-precision microscope measurement machine—MicroVu [32] is used to measure the deformation of the built object. As can be seen from Fig. 6, the 2D profile of the part is a regular shape consists of several rectangles. It would be intuitively to measure the corner points of these rectangles and their edges, and use these corner points to establish the correspondence between nominal model (N) and measured deformed model (M).

The sample points in the nominal model (N) and their correspondences from the measurement of the physical model (M) are plotted in Fig. 8, in which ten points are sampled from each boundary curve, and more points are sampled around corner or position where large deformation gradients exist. User can control the number of sample points. The "*" points denote nominal data, while "+" points denote measured data. From the magnified views of sections (1) and (2), which are picked from the top horizontal plate and the side surface, respectively, it is found that the measured data show the top horizontal plate is curved, while the side surface have dents after built, which agrees with the deformation found on the physical built part.

4 Compensation Calibration and Estimation

The compensation added to the nominal shape will also contribute to the final deformation. This effect makes it difficult to directly compensate the deformation based on the measured errors at each point. In our study, we investigated the relation of added compensation and related deformation based on physical calibrations of offset models. The basic idea is to do a set of experiments with different compensations, i.e., X (X_1, X_2, etc.), and to find out their corresponding deformation ($f(P+X_1)$, $f(P+X_2)$, etc.). With the scattered data in the chart of relationship between compensation and deformation, e.g., $X=0 \leftrightarrow f(P)$, $X=X_1 \leftrightarrow f(P+X_1)$, $X=X_2 \leftrightarrow f(P+X_2)$, we can establish a deformation profile for each point that can be used to find an approximation to the root of Eq. (2).

Parts with simple shapes (e.g., a cylinder or sphere) may have deformation that can be analytically formulated; however, the deformation of more general shapes used in engineering is difficult to be formulated in analytical equations. However, we observed that parts with homogeneous shape (i.e., shapes with the same topology) generally deform in a similar trend with varying deformation sizes. An example is illustrated in Fig. 9, in which a simple bar has double thickness compared with the one shown in Fig. 1. The two parts are built using the same building procedure. Both the parts have the same type of curl distortion; however, the deformation amounts of the surface points are different.

In our study, we make use of offset models, which have the homogeneous shape as the original model. We add compensations at each point on the original nominal model in order to establish the relations between these small offsets and their related deformations. Hence, the additional offset models can be used to calculate the compensation based on the established relations. Two sets of offsets (outward N_+ and inward N_-) are used in this study. Thus, there are three set of data ($X_0=0$, $X_1=N_+$, $X_2=N_-$). More offset models may be used for improved accuracy in compensation calibration and estimation.

Note that the cross-parameterization presented in Sec. 3 is also used to compute the correspondences among all the nominal model (N), measured physical model (M), offset models (N_+, N_-), and their measured physical models (M_+, M_-). Therefore, for each point on the offset and scanned models, it can find the corresponding points on all the related models. Thus, the deformation can be calculated and the comparisons of deformation using offset models can be conducted.

4.1 Using Offset Models for Calibration. The method used in this study is explained as follows:

(1) Build the original nominal model N. For each point P_i on N, find the corresponding point Q_i on the measured model M, and calculate its deformation $f(P_i)$

$$f(P_i) = Q_i - P_i \tag{3}$$

(2) Modify N according to the deformation calculated in step 1 to generate offset models N_+ and N_-. For each point P_i, modify it by offsetting along its normal direction outwardly and inwardly of distance X_1 and X_2, respectively, such that $X_1 < -f(P_i) < X_2$. A corresponding point can be found on N_+ and N_-, denoted as P_i^+ and P_i^-, respectively. Similarly, the corresponding point on measured models M_+, M_- can be found and denoted as Q_i^+ and Q_i^-, respectively.

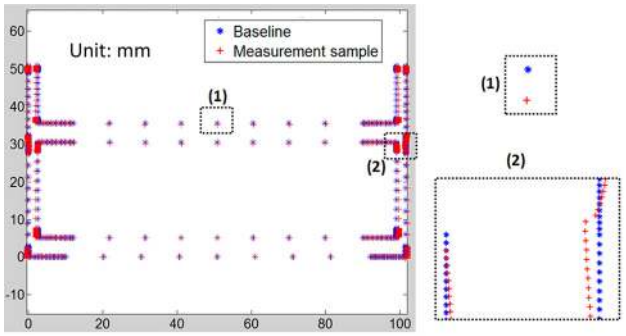

Fig. 8 Sample points of the nominal model and the corresponding points on the physical model

Fig. 9 Simple bar test part with double thickness

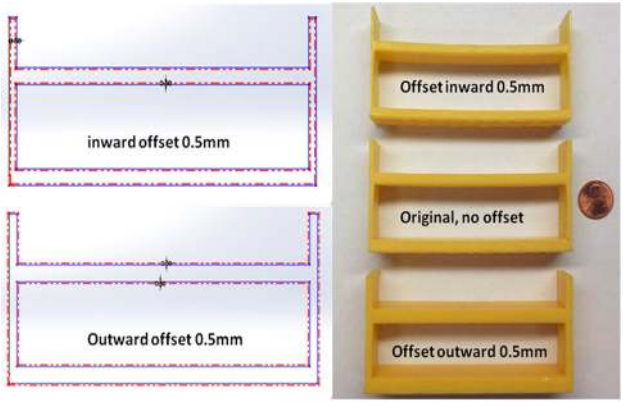

Fig. 10 Offset models and built physical parts

The deformation for each point on the offset models can be calculated as

$$f(P_i + X_1) = Q_i^+ - P_i^+ \tag{4}$$

$$f(P_i + X_2) = Q_i^- - P_i^- \tag{5}$$

(3) From Eqs. (3)–(5), interpolate a value X to get an approximation satisfying $X + f(P + X) = 0$ for each point.

As an illustration, two offset models for modified letter H model are designed by moving every point along its normal direction outwardly and inwardly 0.5 mm, since the physical part has deformation around 0.5 mm. The offset models (N_+, N_-) and physical built parts (M_+, M_-) of the modified letter H model are shown in Fig. 10. The dotted lines show the offset profiles (N_+, N_-), while the solid lines represent original nominal profile (N).

The two offset models are built, measured, and analyzed following the same procedures as the original nominal baseline model (N). After measurements, the same number of sampling points is picked on the offset profiles (N_+, N_-) corresponding to

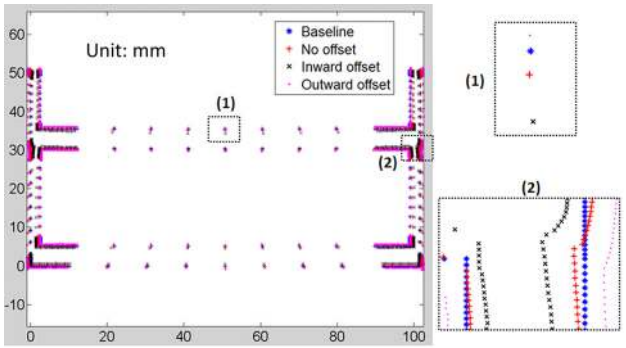

Fig. 11 Comparisons of deformation of models without offset and with offsets

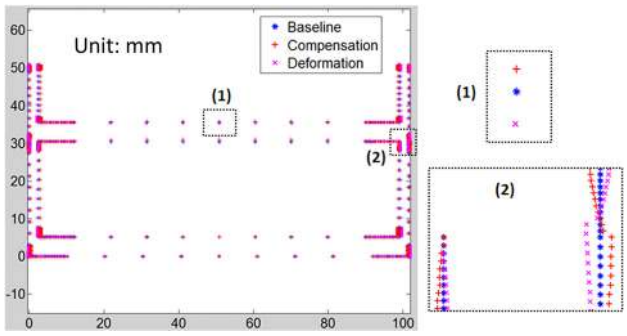

Fig. 12 Compensated profile

that of profile with no offset (N). Deformation for each point on the offset models (N_+, N_-) is calculated by using point in the deformed profiles (M_+, M_-) minus its corresponding point on the nominal profiles (N_+, N_-). The comparisons of measured deformed profiles (M, M_+ and M_-) and original nominal baseline (N) are shown in Fig. 11.

In Fig. 11, the "*" dots show the nominal baseline profile with no offset (N), while the + dots show the deformed profile with no offset (M). The "x" dots show the deformed profile with offset inward 0.5 mm (M_-), and the "." dots show the deformed profile with offset outward 0.5 mm (M_+). From the magnified view of sections (1) and (2), it is found that nominal baseline profile (N) is within the range of deformed profiles with offsets (M_+ and M_-). Therefore, the optimal solution should be within the offset values.

4.2 Establishing Compensation Profile. Compensation for each point is calculated by using three pairs of measured deformation. To calculate the compensation based on these data, we used second-order polynomial to interpolate these data and find the optimal compensation. The compensated profile is shown in Fig. 12. The nominal baseline profile (N) and the original deformation profile with no offset (M) are also plotted in the figure for comparisons. The compensated profile shows in "+" dots, while "*" dots show the nominal profile (N), and "x" dots represent deformed profile (M). Magnified views of a point on the top surface of central plate and a section on the region where dent occurs are drawn to better demonstrate the compensation result (denoted as (1) and (2), respectively). From Fig. 12, it can be seen that the compensated profile is in the reverse direction of deformed profile with respect to nominal profile, and every points on model surfaces have different compensation values, which are calculated from the established compensation profile.

Fig. 13 Compensated STL model

5 Test Results

5.1 Test Case 1—2.5D Freeform Shapes. The modified letter *H* part as shown in Fig. 6 is used as test case 1 for our compensation study. The correspondence between nominal models (*N*) and the measured physical models (*M*), as well as the calculation of the compensation profile, has been explained in Sec. 4. Based on the calculated compensation profile, a modified nominal model is generated (denoted as *C*). The compensated STL model to be fabricated in the test is shown in Fig. 13.

5.1.1 Comparisons of Deformation Before and After Compensation. The compensated STL is built and measured following the same procedure as described in Sec. 4. The measured deformation profile is aligned with nominal baseline profile, and the same number of sampling points is picked from the same positions of the baseline nominal model and the measured profile of the compensated part. The deformation comparison using the compensated STL model (*C*) and the original model without compensation (*N*) are shown in Fig. 14.

Similar to the previous analysis, magnified views of a section on the top surface of central plate and the sidewalls where dents occur are drawn for better illustration. The compensated profile is shown in "." dots, while the original deformed profile is shown in "x" dots, and the "*" dots represent original nominal profile. From the plot, it can be found that the profile using compensated STL model (*C*) is more conformal to the nominal baseline profile (*N*), which suggests the deformation using compensated model (*C*) is much smaller than original model without compensation (*N*). The comparisons of physical built part using compensation and original part are shown in Fig. 15.

To quantitatively characterize the deformation for parts built with and without compensation, we calculate the L^{∞}-norm (max distance) and L^2-norm (root mean squared distance) of the points in nominal profile to the corresponding closest points in the deformed profile, and the results are shown in Table 1.

From Table 1, it can be observed that using the compensated model (*C*) can effectively reduce deformation compared to directly using the nominal model without any compensation (*N*). For the test case, the deformation improvement is 65% and 67% in terms of L^{∞}-norm and L^2-norm, respectively.

5.2 Test Case 2—3D Freeform Shapes. In order to verify the effectiveness of our reverse compensation strategy for more general freeform 3D shape, another test case as shown in

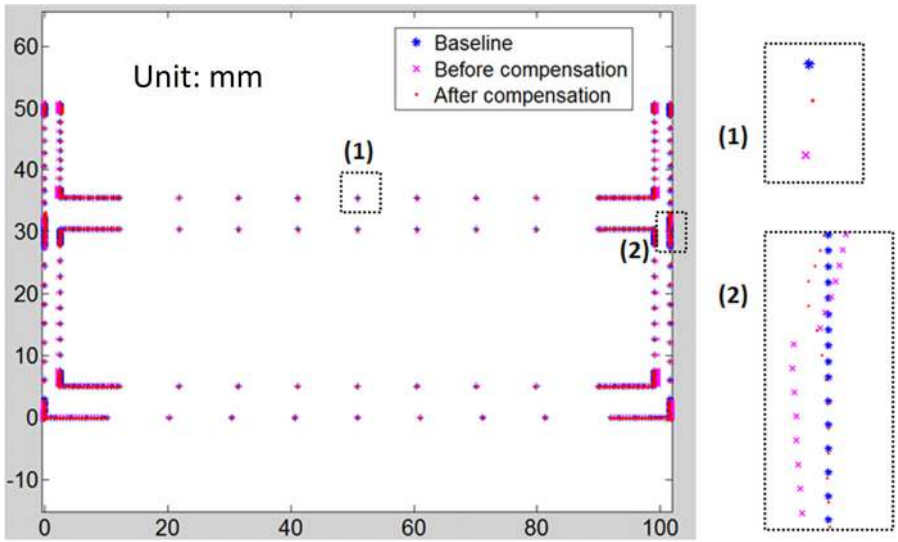

Fig. 14 Comparisons of deformation before and after compensation

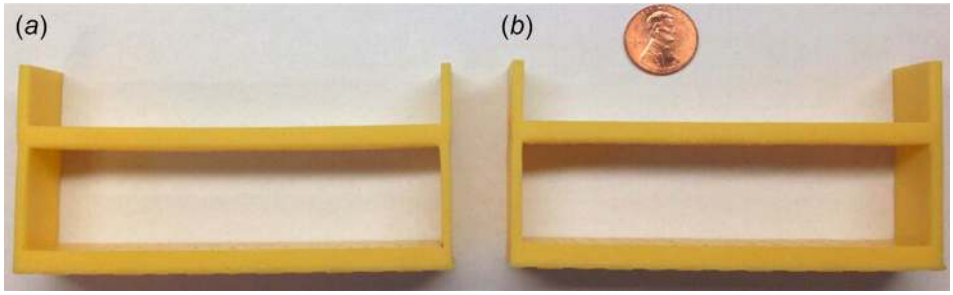

Fig. 15 Comparison of physical built parts: (*a*) original part and (*b*) part with compensation

Table 1 Deformation comparisons before and after compensation for test case 1 (unit: mm)

	Before compensation	After compensation	Improvement (%)
L^{∞}-norm	0.768	0.270	65
L^{2}-norm	0.276	0.090	67

Fig. 16(*a*) was selected to apply the presented computational framework.

The test case is built vertically as shown in Fig. 16(*a*). The built physical part has deformation with two legs spreading out due to the built-up residual stress in the layer-based fabrication process. Such deformation is mainly caused by the shrinkage of the top arch. The shape deformation would be totally different if another building direction is selected.

The nominal dimension between the leftmost point and rightmost point is 51.92 mm. Three-dimensional scanning or related technique can be adopted to measure 3D complex shapes [33,34]. A DAVID-SLS2 3D scanner [35] was used in our study to measure the deformation of built physical parts. The 3D scanner is calibrated before it is used for scanning. As shown in Fig. 16(*a*), test case 2 does not have many salient feature points which can be used for parameterizing the given model. Consequently, small artificial markers were added on model surfaces to assist the parameterization by establishing the correspondence between points on nominal and deformed models.

5.2.1 Deformation Calculations. The baseline nominal model with 35 artificial markers is designed and built using an ultramachine. The nominal STL model (N) and the built physical part are shown in Fig. 4. The built physical part is scanned using the 3D scanner. The two tips of the part are used as the fixture during the scanning process; hence, the related portions are hollow. The related holes can be filled during the mesh fusion process. The 3D scanning result is shown in Fig. 16(*b*), from which it can be seen that there are artificial markers on front and side surfaces. The filled bottom portions are mainly for visualization; they will not be compared with the input nominal model.

The artificial markers on the scanned model can help us to establish the correspondence to the nominal STL model. The positions of these markers on respective mesh model are recorded as specified points. To calculate the deformation of built part, these markers are smoothed and removed from both scanned and original STL models, since they are only designed to establish the correspondence of these two models for mesh parameterization. The specified points on the markers are projected onto the surface of smoothed model. Consistent mesh parameterization of the smoothed scanning model (M) and the nominal STL model (N) without markers can be calculated based on the positions of these 35 corresponding points, similar to those as shown in Fig. 5.

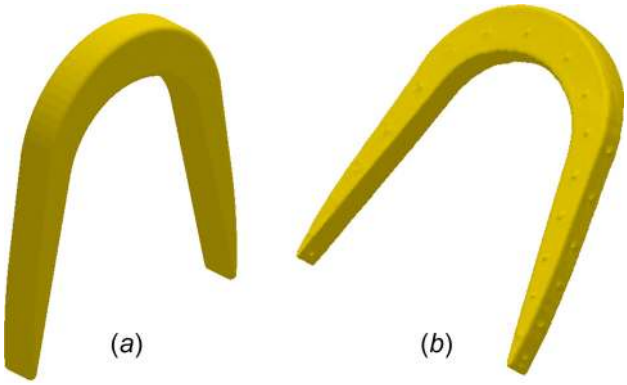

Fig. 16 Testcase 2: (*a*) nominal model and (*b*) scan model with markers

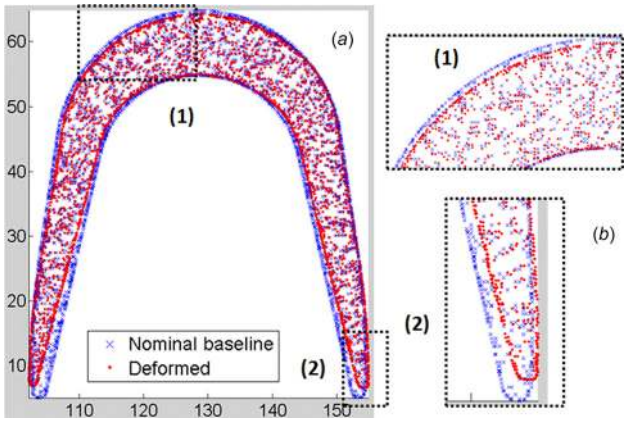

Fig. 17 Comparison of baseline nominal model and scan model compensation: (*a*) comparison of entire model and (*b*) magnified views of two sections

Every vertex in the scanned model (without markers) has a bijective mapping to a vertex in the nominal STL model after parameterization.

The scanned model is then transformed to align with nominal STL model and plotted in Fig. 17(*a*). Magnified views of two sections selected from top and bottom are created for better illustration as shown in Fig. 17(*b*). The "x" dots represent the nominal STL model (N), while the "·" dots show the scanned model (M). From Fig. 17(*b*), it can be clearly seen that the scanned model has deformation with two legs splayed outward. Consequently, the size of the built part changes, which may bring problems if the part needs to be assembled with other parts. Besides, by carefully examine the plot, it can be found that the deformation of left leg and right leg is not symmetric. This slightly nonsymmetric deformation may be generated by the used hardware such as nonuniform light projection. The test case demonstrates the effectiveness of using artificial markers and parameterization to find correspondence between the fabricated part and the nominal model.

5.2.2 Deformation of Offset Models and Analysis. In order to investigate the relations of added compensation and related deformation, two additional models (N_+, N_-) have been designed with offset outwardly 0.5 mm and inwardly 0.5 mm, respectively. These two offset parts were built and scanned using the same parameter settings as the original baseline part. The physical built parts for the two offset models are shown in Fig. 18.

Similar to the parameterization process in baseline model and its scanned model, the nominal offset models (N_+, N_-) and the scanned models (M_+, M_-) are parameterized using the positions of 35 artificial markers on them. The comparisons of the

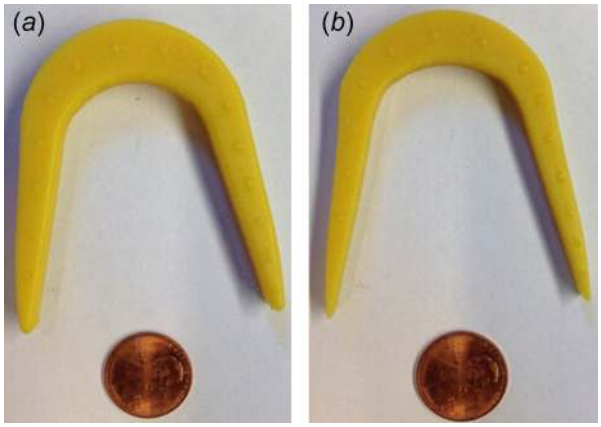

Fig. 18 Physical built parts of offset models

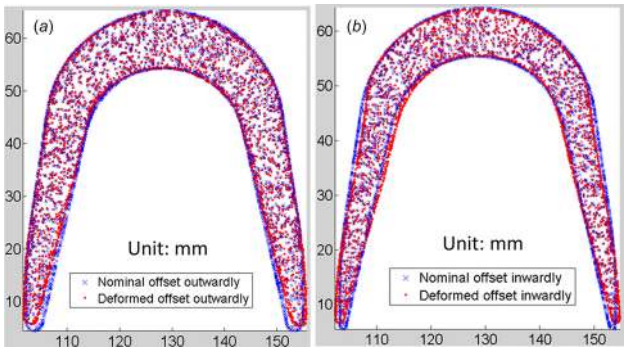

Fig. 19 Deformation using offset models: (*a*) offset outward model and (*b*) offset inward model

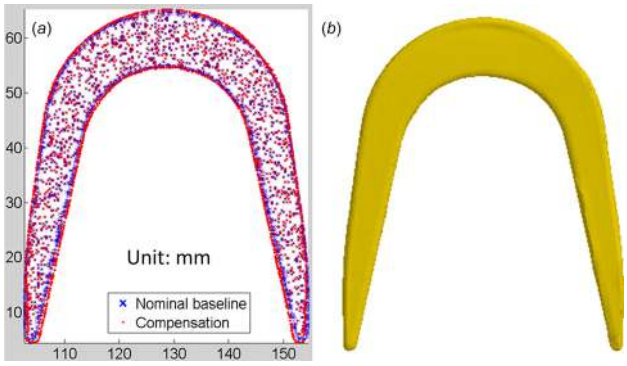

Fig. 20 Compensation: (*a*) compare with nominal model and (*b*) compensated STL model

deformation using the offset models with outward and inward 0.5 mm are plotted in Figs. 19(*a*) and 19(*b*), respectively. In both figures, the "x" dots show the nominal offset models, while the "·" dots represent the deformed models (scanned data). As can be seen from Figs. 17 and 19, all these three test parts (M, M_+, and M_-) follow the same deformation trend with two legs splayed outward and have dents in the center portion of legs.

5.2.3 Reverse Compensation. After mesh parameterization using the artificial markers, all six models (nominal models N, N_+, N_-, and scanned models M, M_+, and M_-) have well-defined correspondence. Each vertex in one model has a unique bijective mapping to a vertex in another model. Therefore, the relations between the deformation and the added offset values for each vertex can be approximated by using the physical parts that were built. Accordingly, the compensation profile can be calculated for each vertex (refer to Eq. (2) in Sec. 2). The calculated compensation and accordingly compensated STL model are shown in Figs. 20(*a*) and 20(*b*), respectively. In Fig. 20(*a*), the compensation profile is shown in "x" dots, while the nominal model is shown in "·" dots, from which it can be found that the compensation is in the reverse direction as original deformation shown in Figs. 17 and 19. Using the compensation profile, the nominal model can be easily modified with compensation added on it and exported as the compensated STL model.

5.2.4 Deformation Comparisons. The compensated STL model is built with 35 artificial markers added on it and then measured using the 3D scanner. The scanned model is compared with the nominal model following the same procedure as described before. The comparisons of physical part with and without the added compensation are shown in Fig. 21.

The deformation of physical part with compensation is calculated by comparing the nominal STL model and the scanned model, as shown in Fig. 22. Magnified views of two select

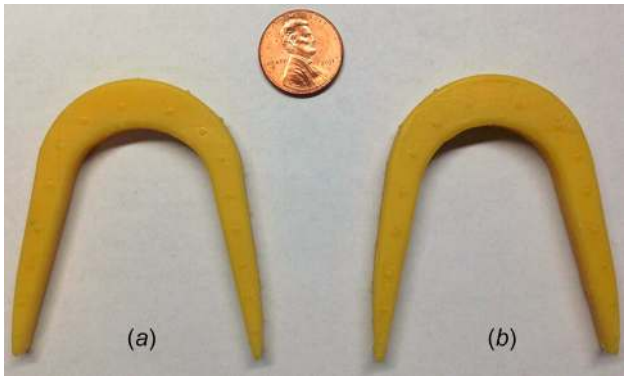

Fig. 21 Physical parts comparisons: (*a*) without compensation and (*b*) with compensation

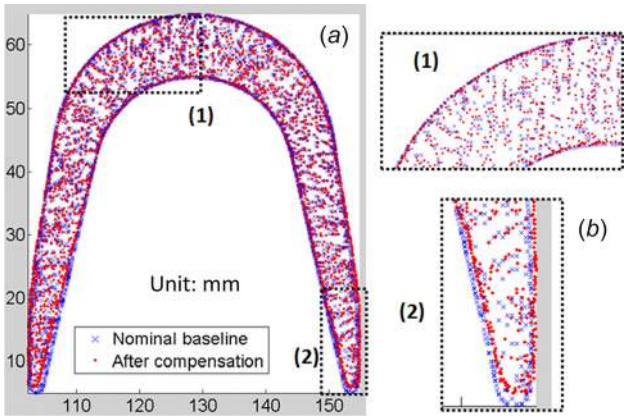

Fig. 22 Deformation of built part with compensation: (*a*) comparison of entire model and (*b*) magnified views of two sections

Table 2 Deformation comparisons before and after compensation for test case 2 (unit: mm)

	Before compensation	After compensation	Improvement (%)
L^∞-norm	2.240	1.300	42
L^2-norm	0.692	0.3111	55

sections on the top and bottom are created for better illustration. Compared to Fig. 17, it can be found that the part built with compensation has much less deformation than the original nominal shape.

Similar to test case 1, the deformation of physically built objects with and without compensation are quantitatively compared. L^∞-norm (max distance) and L^2-norm (root mean squared distance) of all the points in the nominal model to corresponding closest points in the deformed model (in the XZ plane) are calculated for both parts and shown in Table 2. The L^∞-norm of deformation before and after using the compensation is 2.24 mm and 1.3 mm, respectively, with deformation improvement around 42%. The L^2-norm of deformation without compensation is 0.692 mm, while the L^2-norm of deformation with compensation is 0.311 mm, which shows that the added compensation can have around 55% improvement on shape deformation.

6 Conclusions

In this paper, we present a general computational framework based on reverse compensation to reduce the complex

deformation that may happen in additive manufacturing processes. Corresponding points between nominal and deformed shapes are found by applying cross-parameterization using a set of feature points. Such feature points could be the existing salient features on the model or the artificial markers that are added on 3D free-form surfaces. By studying the relation of offset models and related deformation for surface points, the reverse compensation profile can be established. Two test cases have been presented to demonstrate the capability of the developed computational framework. The final compensated STL models have been built and compared with the original models. It is found that the compensated models can significantly reduce the shape deformation for both test cases.

Currently, we apply our reverse compensation only once. The accuracy can be further improved by iteratively applying the compensation. However, our method requires the fabrication of the nominal and the offset models, which makes the iteration expensive. We plan to integrate a simulation framework with physical experiments such that the deformation can be predicted by simulation with less physical tests that are required. Another limitation of our method is that the measurement error cannot be compensated. Currently, the measurement error due to the used 3D scanner is around 0.2–0.3 mm, which is much smaller than the deformation of the test part.

In the future, we plan to apply the computational framework to more general 3D test cases. In addition, we will study how to add artificial markers that are more effective in registration and finding correspondence between measured and nominal models. More intelligent offsetting strategies for compensation calibration will also be investigated.

Acknowledgment

The work is partially supported by Office of Naval Research with Grant No. N000141110671 and NSF Grant No. CMMI 1333550. We also acknowledge the help of Professor Qiang Huang at USC and Mr. Leu-Yang Eric Huang, a high school summer intern, on 3D scanning study.

References

[1] Optical Sciences Corporation, 2016, "Overview of the Digital Micromirror Device," Optical Sciences Corporation, Huntsville, AL, accessed Aug. 21, 2016, http://www.opticalsciences.com/dmd.html
[2] Zhou, C., Chen, Y., and Waltz, R. A., 2009, "Optimized Mask Image Projection for Solid Freeform Fabrication," ASME J. Manuf. Sci. Eng., **131**(6), p. 061004.
[3] EnvisionTEC, 2012, "Ultra Machine," EnvisionTEC, Dearborn, MI, accessed Jan. 20, 2012, http://www.envisiontec.de/index.php?id=108
[4] Limaye, A. S., and Rosen, D. W., 2007, "Process Planning Method for Mask Projection Micro-Stereolithography," Rapid Prototyping J., **13**(2), pp. 76–84.
[5] Zhou, C., and Chen, Y., 2012, "Additive Manufacturing Based on Optimized Mask Video Projection for Improved Accuracy and Resolution," J. Manuf. Processes, **14**(2), pp. 107–118.
[6] Pan, Y., Zhou, C., and Chen, Y., 2012, "A Fast Mask Projection Stereolithography Process for Fabricating Digital Models in Minutes," ASME J. Manuf. Sci. Eng., **134**(5), p. 051011.
[7] Zhou, C., Ye, H., and Zhang, F., 2015, "A Novel Low-Cost Stereolithography Process Based on Vector Scanning and Mask Projection for High-Accuracy, High-Speed, High-Throughput, and Large-Area Fabrication," ASME J. Comput. Inf. Sci. Eng., **15**(1), p. 011003.
[8] Jacobs, P. F., 1992, *Rapid Prototyping and Manufacturing: Fundamentals of Stereolithography*, Society of Manufacturing Engineers, Dearborn, MI.
[9] Huang, Y. M., and Jiang, C. P., 2003, "Curl Distortion Analysis During Photopolymerisation of Stereolithography Using Dynamic Finite Element Method," Int. J. Adv. Manuf. Technol., **21**(8), pp. 586–595.
[10] Guess, T. R., Chambers, R. S., Hinnerichs, T. D., McCarty, G. D., and Shagam, R. N., 1995, "Epoxy and Acrylate Stereolithography Resins: In-Situ Measurements of Cure Shrinkage and Stress Relaxation," Sandia National Labs, Albuquerque, NM, Report Nos. SAND–94-2569C.
[11] Narahara, H., Tanaka, F., Kishinami, T., Igarashi, S., and Saito, K., 1999, "Reaction Heat Effects on Initial Linear Shrinkage and Deformation in Stereolithography," Rapid Prototyping J., **5**(3), pp. 120–128.
[12] Hur, S. S., and Youn, J. R., 1998, "Prediction of the Deformation in Stereolithography Products Based on Elastic Thermal Shrinkage," Polym.-Plast. Technol. Eng., **37**(4), pp. 539–563.
[13] Xu, K., and Chen, Y., 2014, "Curing Temperature Study for Curl Distortion Control and Simulation in Projection Based Stereolithography," ASME Paper No. DETC2014-34908.
[14] Xu, K., and Chen, Y., 2014, "Deformation Control Based on In-Situ Sensors for Mask Projection Based Stereolithography," ASME Paper No. MSEC2014-4055.
[15] Vatani, M., Barazandeh, F., Rahimi, A., and Nezhad, A. S., 2012, "Distortion Modeling of SL Parts by Classical Lamination Theory," Rapid Prototyping J., **18**(3), pp. 188–193.
[16] Davis, B. E., 2001, "Characterization and Calibration of Stereolithography Products and Processes," Doctoral dissertation, Georgia Institute of Technology, Atlanta, GA.
[17] Huang, Y. M., and Lan, H. Y., 2006, "Path Planning Effect for the Accuracy of Rapid Prototyping System," Int. J. Adv. Manuf. Technol., **30**(3–4), pp. 233–246.
[18] Xu, K., and Chen, Y., 2015, "Mask Image Planning for Deformation Control in Projection-Based Stereolithography Process," ASME J. Manuf. Sci. Eng., **137**(3), p. 031014.
[19] Campanelli, S. L., Cardano, G., Giannoccaro, R., Ludovico, A. D., and Bohez, E. L., 2007, "Statistical Analysis of the Stereolithographic Process to Improve the Accuracy," Comput.-Aided Des., **39**(1), pp. 80–86.
[20] Onuh, S. O., and Hon, K. K. B., 2001, "Improving Stereolithography Part Accuracy for Industrial Applications," Int. J. Adv. Manuf. Technol., **17**(1), pp. 61–68.
[21] Bugeda, G., Cervera, M., Lombera, G., and Onate, E., 1995, "Numerical Analysis of Stereolithography Processes Using the Finite Element Method," Rapid Prototyping J., **1**(2), pp. 13–23.
[22] Huang, Y. M., and Lan, H. Y., 2005, "Dynamic Reverse Compensation to Increase the Accuracy of the Rapid Prototyping System," J. Mater. Process. Technol., **167**(2), pp. 167–176.
[23] Tong, K., Lehtihet, E. A., and Joshi, S., 2003, "Parametric Error Modeling and Software Error Compensation for Rapid Prototyping," Rapid Prototyping J., **9**(5), pp. 301–313.
[24] Zha, W., and Anand, S., 2015, "Geometric Approaches to Input File Modification for Part Quality Improvement in Additive Manufacturing," J. Manuf. Processes, **20**(3), pp. 465–477.
[25] Huang, Q., Zhang, J., Sabbaghi, A., and Dasgupta, T., 2015, "Optimal Offline Compensation of Shape Shrinkage for Three-Dimensional Printing Processes," IIE Trans., **47**(5), pp. 431–441.
[26] Huang, Q., Nouri, H., Xu, K., Chen, Y., Sosina, S., and Dasgupta, T., 2014, "Statistical Predictive Modeling and Compensation of Geometric Deviations of Three-Dimensional Printed Products," ASME J. Manuf. Sci. Eng., **136**(6), p. 061008.
[27] Huang, Q., 2016, "An Analytical Foundation for Optimal Compensation of Three-Dimensional Shape Deformation in Additive Manufacturing," ASME J. Manuf. Sci. Eng., **138**(6), p. 061010.
[28] Besl, P. J., and McKay, N. D., 1992, "A Method for Registration of 3-D Shapes," IEEE Trans. Pattern Anal. Mach. Intell., **14**(2), pp. 239–256.
[29] van Kaick, O., Zhang, H., Hamarneh, G., and Cohen-Or, D., 2011, "A Survey on Shape Correspondence," Comput. Graphics Forum, **30**(6), pp. 1681–1707.
[30] Kwok, T. H., Zhang, Y., and Wang, C. C., 2012, "Constructing Common Base Domain by Cues From Voronoi Diagram," Graphical Models, **74**(4), pp. 152–163.
[31] Kwok, T. H., Zhang, Y., and Wang, C. C. L., 2012, "Efficient Optimization of Common Base Domains for Cross Parameterization," IEEE Trans. Visualization Comput. Graphics, **18**(10), pp. 1678–1692.
[32] Micro-Vu Corporation, 2016, "MicroVu Measurement Machine," Micro-Vu Corporation, Windsor, CA, accessed on July 16, 2016, http://www.microvu.com/sol.html
[33] Chen, Y., Li, K., and Qian, X., 2013, "Direct Geometry Processing for Telefabrication," ASME J. Comput. Inf. Sci. Eng., **13**(4), p. 041002.
[34] Kaufman, J., Clement, M., and Rennie, A. E., 2015, "Reverse Engineering Using Close Range Photogrammetry for Additive Manufactured Reproduction of Egyptian Artifacts and Other Objets d'art," ASME J. Comput. Inf. Sci. Eng., **15**(1), p. 011006.
[35] David Vision Systems GmbH, 2016, "SLS-2 Structured Light 3D Scanner," Koblenz, Germany, accessed on Aug. 21, 2016, http://www.david-3d.com/en/products/sls-2